Nanoperforated Polyester Nanomembranes as Templates of Electroactive and Robust Free-standing Films

Brenda G. Molina,[1,2,*] *Sergi Cuesta,*[1] *Anna Puiggalí-Jou,*[1,2]

Luis J. del Valle,[1,2] *Elaine Armelin,*[1,2,*]

and Carlos Alemán[1,2,*]

[1] *Departament d'Enginyeria Química, EEBE, Universitat Politècnica de Catalunya, C/ Eduard Maristany, 10-14, Ed. I2, 08019, Barcelona, Spain*

[2] *Barcelona Research Center for Multiscale Science and Engineering, Universitat Politècnica de Catalunya, C/ Eduard Maristany, 10-14, Ed. C, 08019, Barcelona, Spain*

[*] Correspondence to: brenda.guadalupe.molina@upc.edu, elaine.armelin@upc.edu and carlos.aleman@upc.edu

ABSTRACT

Robust and flexible free-standing films made of spin-coated poly(lactic acid) (PLA) and poly(3,4-ethylenedioxythiophene) (PEDOT) nanolayers have been prepared. A steel sheet coated with a sacrificial layer of PEDOT:poly(styrenesulfonate) (PSS) and a spin-coated nanolayer of PLA was used as working electrode for the anodic polymerization of 3,4-ethylenedioxythiophene monomer. The latter was only successfully accomplished when rounded-shape nanoperforations of average diameter 49±14 nm were introduced into PLA layers, which was achieved by combining the phase segregation processes undergone by immiscible PLA:poly(vinyl alcohol) (PVA) mixtures with selective solvent etching to remove PVA domains. Nanoperforations allowed the utilization of the semiconducting PEDOT:PSS sacrificial layer to immobilize the electropolymerized PEDOT chains. Morphological and topographical studies show the templating effect of PEDOT layers. In addition of flexibility and mechanical strength, free-standing 5-layered films present good electrochemical activity, evidencing their potential ability to reversibly exchange ions with the medium. These properties offer important advantages with respect to those of neat PLA and supported PEDOT films, as has been illustrated by cell culture and protein adsorption assays. Cell cultures evidenced the superior behavior of 5-layered films as bioactive platforms for fibroblast and epithelial cells proliferation, while adsorption assays reflected their potential as selective bioadhesive surfaces for protein separation.

Keywords: giant nanomembranes; nanofeature; phase segregation; self-supported films; tissue engineering

INTRODUCTION

In the last decade nanotechnology concepts and nanomaterials have been applied to obtain and improve devices with very different applications in biomedicine and biotechnology [1-5]. Within this context, there is a growing interest in the fabrication of nanomembranes (also known as ultra-thin films or nanosheets) because their distinctive features make them suitable for their use as sensors [6,7], biomotors [8], biointerfaces for cellular matrices [9-11], antimicrobial surfaces [12,13], and drug release devices [14,15].

The term *nanomembrane* typically refers to quasi-2D structures with macroscopic surface area and nanoscale thickness (*i.e.* from 10 to a few hundreds of nanometers). A decade ago Kunitake [16], one of the pioneers in the field, coined the term "*giant nanomembrane*" to denote self-supported, also named free-standing, nanomembranes with an aspect ratio of size and thickness greater than 10^6. This aspect ratio facilitates the macroscopic use of nanomembranes while the self-supporting property, which enables the nanomembrane to retain its mechanical integrity when it is removed from the substrate, is required to physically separate two spaces. Overall, these characteristics confer special properties to free-standing nanomenbranes (hereafter denoted FsNMs), such as: low weight, high flexibility and robustness [17]. The seminal features and characteristics of FsNMs technology, including fabrication methods, mechanical properties and health-care applications (*e.g.* as wound dressings, tissue engineering materials and bioelectronic devices) have been recently reviewed [18-20].

Although single-layered FsNMs have been widely developed and employed during the last years, the utilization of polymeric multi-layered FsNMs (hereafter ml-FsNMs) has been much less explored despite the advantages of this approach [18-20]. The layer-by-layer (LbL) assembly [21,22], which is based on the deposition alternating layers of

oppositely charged materials onto a solid surface, is probably the most simple technique for the preparation of ml-FsNMs. However, the thickness of the resulting free-standing polymer films, which is 10-15 nm only [23], represents an important limitation for their manipulation and, therefore, for their practical application. Spin-coating represents an interesting alternative to LbL technique since ml-FsNMs with higher mechanical strength could be produced in a few steps. Optimization of the spin-coating parameters (*e.g.* spinning speed, spinning time and the polymer solution concentration) typically results in homogenous polymeric films with controlled thickness. In this approach, the liquid solution of the polymer is spin casted onto a solid substrate, which has been previously coated with a sacrificial layer. For the preparation of multi-layered films, the spin-coating process is repeated as many times as layers wants to accumulate and, finally, the sacrificial layer is dissolved in an appropriated solvent to achieve the detachment of the ml-FsNM.

In a recent but pioneering study [24], the spin-coating multi-layering process was used to prepare multilayered films of poly(vinyl alcohol) (PVA) and poly(lactic acid) (PLA). These were transformed into suspended PLA nanomembranes, which subsequently patched into a continuous film, by dissolving the sacrificial PVA layers between PLA layers. Since then, the spin-coating multi-layering process has been combined with other approaches, such as LbL and chemical cross-linking of assembled layers, to produce supported multi-layered polymeric films for biomedical applications (*e.g.* drug release and antimicrobial surfaces) [25-28]. However, the preparation and application of polymeric ml-FsNMs is a challenge yet.

In this work we explore the spin-coating technique alone and combined with the *in situ* anodic polymerization (AP) for the preparation of 5-layered FsNMs made of alternated layers of PLA and a conducting polymer (CP). Specifically, films consisting in

three spin-coated PLA layers separated by two spin-coated CP layers (5-PLA/CP_{SC}, where CP_{SC} indicates that the CP has been deposited by spin-coating) and films consisting of three spin-coated non-perforated or perforated PLA layers separated by two layers of CP deposited by *in situ* AP (5-PLA/CP_{AP} and 5-pPLA/CP_{AP}, respectively, where CP_{AP} indicates that the CP has been deposited by AP and pPLA refers to perforated PLA) have been tried (Scheme 1). It should be noted that the choice in the number of 5 layers, which was performed after some preliminary tests, obeys to the compromise between good properties and the operational difficulties associated with the preparation of multilayer systems that requires a long and tedious process. The CP used in this work is poly(3,4-ethylenedioxythiophene), abbreviated PEDOT, which is frequently employed for the fabrication of biomedical devices because of its outstanding electrochemical properties, biocompatibility and stability in continuous operation [29-31]. Furthermore, this CP was found to be very effective for the electro-stimulated release of encapsulated drugs [32]. Although the preparation of 5-PLA/CP_{SC} and 5-PLA/CP_{AP} presented serious limitations, the appropriate use of such drawbacks has been successful in the design, fabrication and proper application of 5-pPLA/CP_{AP} FsNMs.

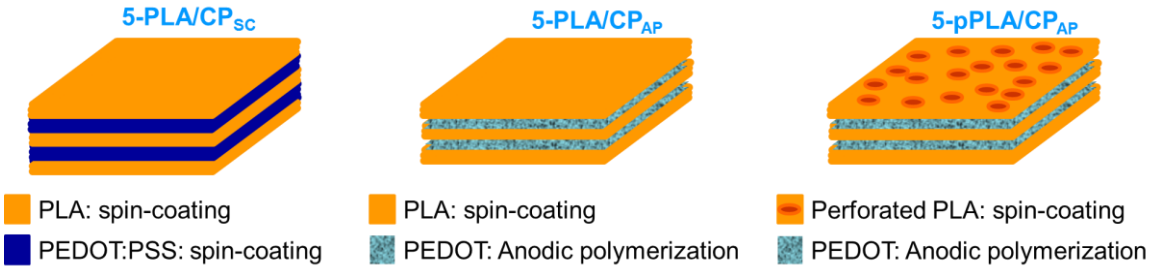

Scheme 1: Schematic representation of the three 5-layered films tried in this work.

RESULTS AND DISCUSSION

Preparation of 5-PLA/CP_{SC}

Among the synthetic polymers used to prepare FsNMs for biomedical applications, linear aliphatic polyesters, such as biocompatible PLA, have been extensively chosen since their biodegradation rate, mechanical properties and adhesion strength, can be easily controlled through variations in their molecular weight [24,33-37]. For the fabrication of PLA layers, a 10 mg/mL polymer solution in chloroform was spin-coated at angular speeds of 1200, 2500, 5000 and 7000 rpm for 1 min to obtain nanomembranes onto a glass substrate. As it was expected, the variation of the thickness of the resulting films was inversely proportional to the speed, being 110±8, 89±6, 73±9 and 61±5 nm, respectively. Among the tested conditions, a speed of 1200 rpm, which produced the thickest nanomembrane, was selected for all spin-coated PLA films.

On the other hand, a commercial (1.3 wt. %) stable aqueous dispersion of PEDOT with excess of poly(styrenesulfonate) (PEDOT:PSS) was used to prepare spin-coated PEDOT layers. It is worth noting that only 2% of the sulfonate groups of PSS interact with PEDOT acting as dopant, the other 98% being employed as a rheological additive to increase the viscosity of the dispersion [29]. The PEDOT:PSS aqueous dispersion was spin-coated at 1200, 2500, 5000 and 7000 rpm for 1 min. Homogeneous thin films were only obtained at the two former angular speeds, their thickness being 173±19 and 80±8 nm, respectively. As in the case of PLA, the lowest angular speed was selected for the preparation of 5-PLA/CP_{SC} films since the mechanical consistency was expected to improve with increasing film thickness.

The fabrication of 5-PLA/CP_{SC} films was tried by spin-coating three PLA and two PEDOT:PSS layers alternatively (Scheme 1). Unfortunately, the deposition of the CP onto the first PLA layer was not achieved because of the poor hydrophilicity of the latter material (water contact angle, WCA: 72º±4º), which caused the expulsion of the PEDOT:PSS drop when applying the angular speed (Figure S1). In order to overcome

this drawback, a surface treatment was applied to increase the hydrophilicity of the PLA layer [38]. More specifically, an aliquot of a 0.5 M NaOH solution was dropped onto the surface of PLA layer for 30 min and, subsequently, it was gently washed with water. A decrease in the water contact angle (WCA) from 72º±4º to 22º±5º at PLA surface, was achieved due to the hydrolytic cleavage of ester bonds and the generation of carboxylate groups. Although this surface activation treatment was successfully used to prepare 3-layered PLA/PEDOT:PSS/PLA films, it failed for 5-layered films due to the solubilization of intermediate PEDOT:PSS layer during the water washing step of the third PLA layer previous to the deposition of the fourth layer (Figure S2). Accordingly, PLA functionalization is not a suitable strategy for the preparation of multi-layered PLA/CP_{SC} films with more than 3-layers. Despite the limitation, these results were used for the correct design of 5-pPLA/CP_{AP} FsNMs (see below).

Preparation of non-perforated 5-PLA/CP_{AP} and perforated 5-pPLA/CP_{AP}

Deposition of PEDOT layers by *in situ* AP of 3,4-ethylenedioxythiophene (EDOT) monomers onto PLA layers was considered as an alternative approach to spin-coated PEDOT:PSS layers. In order to test this strategy, a PLA layer, spin-coated onto steel substrate (AISI 316L sheet of 1×2 cm^2), was used as working electrode for the setup used in the electropolymerization of EDOT (see Methods section in the Supplementary Information). Although it is an insulating polymer, the diffusion of small and medium size molecules across PLA nanostructures (*i.e.* nanofilms and nanofibers) has been reported [39], and therefore, the PEDOT nanolayer could be successfully obtained (Figure S3). Nevertheless, the thickness and aspect of the CP film were not homogenous, which represented a significant drawback with respect to films generated directly onto

bare steel electrodes. This fact was attributed to the influence of microstructure of the PLA layer on the AP process.

In order to overcome this limitation, a physical modification was introduced in the spin-coated PLA layers. More specifically, PLA layers with nanopores crossing the entire thin-film thickness were prepared using spin-coating combined with phase segregation processes in immiscible PLA:PVA mixtures and, subsequently, removing PVA domains via solvent etching [11]. This process, which is schematically illustrated in Figure 1a and is fully described in the Methods section (Supplementary Information), was achieved by spin-coating mixtures of PLA and PVA solutions in 1,1,1,3,3,3-hexafluoro-2-propanol (HFIP). Besides, 5-pPLA/CP_{AP} films were prepared by combining such process with the AP of EDOT, as is shown in Figure 1b.

Morphology, topography and wettability of 5-pPLA/CP_{AP} films

Figure 2a displays a representative SEM micrograph and both 3D topographic and height AFM images of the nanoperforated PLA film spin-coated onto a steel substrate. The average diameter of the nanoperforations, which are rounded-shape, is 49±14 nm as determined from SEM micrographs. The root-mean-square roughness (Rq) increased from 1.7±0.2 nm for non-perforated PLA (Figure S4) to 6±1 nm after removal of PVA domains via selective solvent etching, while the thickness increases from 110±8 and 114±11 nm.

AP of EDOT onto the first perforated PLA layer resulted in a cohesive bilayer with the CP adhered to the polyester (Figure 1b). This is also evidenced in Figure 3a, which shows a micrograph of an intentionally scratched 2-layered film to observe both, the PLA and PEDOT sides. On the other hand, Figures 2b-2e successively display the surface morphology and topography of the 2^{th} (PEDOT), 3^{rd} (perforated PLA), 4^{th} (PEDOT) and

5th (perforated PLA) layers. As it can be seen, the shape and diameter of the nanoperforations are affected by the PEDOT intermediate layers. Specifically, nanoperforations becomes bigger (76±27 and 103±40 nm for the 3rd and 5th layer, respectively) and more irregular than in the 1st layer. These observations have been attributed to surface morphology of PEDOT layers, which affects the distribution of PLA:PVA phases during the spin-coating process. Thus, PEDOT presents a globular morphology in which the CP chains grow forming small clusters that affect the size of PVA nanophases during the spin-coating of the PLA:PVA mixture. Obviously, the globular morphology of PEDOT, which presents a Rq substantially higher than that of spin-coated PLA, affects the 3rd and 5th layers (Figure 3b). Thus, the Rq of PLA layers increases from 6±1 nm (1st) to 90±14 and 103±9 nm (3rd and 5th, respectively). The progressive enhancement of this template effect correlates with the Rq of the 2nd and 4th PEDOT layers (138±17 and 312±14 nm, respectively

Figure 3c displays the thickness of each layer in the 5-pPLA/CP_{AP} determined by scratching the films and measuring the step values with AFM and contact profilometry, respectively. As it can be seen, the two methodologies provide consistent results. The thickness of the whole 5-layered film is around 0.7 μm, which is distributed in ~0.4 μm and ~0.3 μm for the two PEDOT and three PLA layers, respectively. Interestingly, the thickness the 3rd and 5th PLA layers decreases by ~20% with respect to the 1st layer, which has been also attributed to the templating effect exerted by PEDOT globules.).

The water contact angle (WCA) was determined for each layer of 5-pPLA/CP_{AP} films supported onto steel (Figure 3d). Results indicate that the poor hydrophilicity of PLA, which exhibits WCA values relatively close to 90º (*i.e.* from 78º±4º to 84º±5º) and the very remarkable hydrophilicity of PEDOT (*i.e.* 46º±6º and 49º±8º for the 2nd and 4th layer, respectively) are practically independent of the layer. Besides, the effect of

nanoperforations in the reduction of wettability is small, the WCA of non-perforated PLA films was found to be 72º±4º.

Preparation of 5-pPLA/CP_{AP} FsNMs

The preparation of 5-pPLA/CP_{AP} FsNMs requires the utilization of a sacrificial layer onto the steel substrate, which will be subsequently dissolved to detach the 5-layered film. Although PVA is typically used as sacrificial layer because of its solubility in water, in this case its utilization was not feasible. Insulating PVA precluded the AP of EDOT for the 2nd PEDOT layer, hindering the action of the steel working electrode in the AP process. In order to overcome this drawback, we took advantage of the experience acquired during the unsuccessful preparation of 5-PLA/CP_{SC} films. More specifically, we used a water dispersion of PEDOT:PSS to prepare an electroactive sacrificial layer onto the steel sheet by spin-coating. The thickness and Rq of this sacrificial layer, which was obtained applying a spinning speed of 1200 rpm for 60 s, was 163±3 and 7±1 nm, respectively. Furthermore, the previously discussed incompatibility between hydrophilic PEDOT:PSS (WCA: 36º±5º) and hydrophobic PLA was not detected when the 90:10 PLA:PVA v/v mixture was spin-coated onto the sacrificial layer due to the beneficial hydrophilicity of PVA.

The deposition of the three nanoperforated PLA layers and the two PEDOT layers was performed as was illustrated previously (Figure 1b). PVA etching after spin-coating the PLA:PVA mixture was carried out by covering the surface of the layer with a drop of milli-Q water and , therefore, avoiding any undesired effect in the stability of the PEDOT:PSS sacrificial layer. Photographs displaying the aspect of the film after the deposition of each spin-coated or anodically polymerized layer are provided in Figure 4a, while a 5-pPLA/CP_{AP} of 9 cm^2 area is shown in Figure 4b. Detachment of the 5-

pPLA/CP_{AP} film from the steel substrate was achieved by immersion into milli-Q water for 12 h. After this time, a pair of tweezers was used to completely detach the 5-layered film.

Self-standing 5-pPLA/CP_{AP} films are very flexible and robust, their folding into small shapes being an easy process. This is evidenced in Figure 4c, which show digital camera images of the aspiration of a film with an area of 1 cm^2 floating in water into a pipette with a tip diameter of 1 mm. As it can be seen, the film is completely introduced into the pipette due to its outstanding flexibility. After releasing it into a solvent, the film recovers immediately without need of any manipulation. This aspiration/shape recovery process can be repeated more than five times without producing any damage in the film. The mechanical strength of 5pPLA/CP_{AP} films was estimated by picoindentation measurements (Figure S5) that revealed an elastic modulus of 2.5 GPa. This value is slightly lower than that typically reported for bulk PLA (3.0-3.5 GPa), which has been attributed to the poor mechanical properties of CP layers when produced by AP.

Chemical characterization by Raman spectroscopy of the whole 5-pPLA/CP_{AP} system is provided in Figure 4d, which displays the spectra of the film as it grows layer-by-layer from the sacrificial layer to the 5^{th} PLA layer. The Raman fingerprints of PEDOT were reported in previous studies [40,41]. The main vibrational mode of PEDOT layers at 1424 cm^{-1}, the less intense band at 1364 cm^{-1}, and the shoulder at 1490 cm^{-1} correspond to the symmetric C_α=C_β stretching, C_α–$C_{\alpha'}$ inter-ring stretching vibrations, and asymmetric C_α=C_β stretching, respectively. Other important bands appear at 856 and 991 cm^{-1} which have been attributed to the asymmetric C–S–C deformation and O–C–C–O ring deformation, respectively. Furthermore, the intensity of these fingerprint bands increases with the number of PEDOT layers, confirming the successful incorporation of electrochemically polymerized PEDOT.

Raman spectra of PLA layers are highly similar to those of PEDOT layers (Figure 4d) due the lower content of the former polymer (*i.e.* the thickness of PLA layers was 2-3 times smaller than that of PEDOT layers, as shown in Figure 3c), and the superposition of the most characteristic bands was observed. Furthermore, the predominance of PEDOT bands in the 5-layered system can be also attributed to the resonance Raman effect, which increases the intensity of the bands of the material when the laser energy coincides with the frequency of the electronic transition of the sample [42,43]. Further studies were carried out to understand the compositional distribution of 5-pPLA/CP_{AP} films by means of FTIR spectroscopy, which is more appropriate for the structure elucidation of polar groups. Results are discussed in the Supporting Information (Figure S6).

Cell cultures

In this section we examine the effects of the possible synergies between PLA and PEDOT layers in the biocompatibility of these materials. For this purpose, Cos-1 and Vero cells, which are green monkey kidney fibroblast and epithelial cells, respectively, were used for cell adhesion and cell proliferation studies conducted on PLA and PEDOT films supported on steel, 5-pPLA/CP_{AP} FsNMs and bare steel sheets (control). The cell viability was evaluated by the MTT [3-(4,5-dimethylthiazol-2-yl)-2,5-diphe-nyltetra-zolium] method after 24 hours (cell adhesion) and 7 days (cell proliferation) of incubation. Figure 5a shows that, in appearance, adhesion of cells preferably occurs onto PLA and 5-pPLA/CP_{AP} films, even though differences are statistically unmeaning (Student's T-test with $p< 0.05$). Figure 5b indicates that cell proliferation is slightly greater for supported PEDOT and 5-pPLA/CP_{AP} FsNMs than for bare steel sheets and nanoperforated PLA films, even though significant differences with *p*-values lower than

0.05 were not detected when the Student's T-test was applied. These results reflect that 5-pPLA/CP_{AP} films are able to capture the advantages of both PLA and PEDOT (*i.e.* mechanical strength and ability to exchange ions with cells, respectively).

On the other hand, micrographs of the films cultured for 24 hours and 7 days are displayed in Figure 5c. It is worth noting that in all cases cells exhibited a healthy morphology in terms of shape and appearance (*i.e.* no sign of detachment of the cells from the substrate was detected). Cos-1 cells display elongated shapes and are spindle-shaped (bipolar) or stellate-shaped (multipolar), whereas Vero cells show more regular dimensions and grow attached to the substrate in discrete patches. These *in vitro* cell assays evidence that PLA and PEDOT containing 5-layered FsNMs favor the growth of fibroblast and epithelial cells by combining the best properties of each individual polymer in a single bioplatform.

Protein adsorption

In order to evaluate the ability of 5-pPLA/CP_{AP} FsNMs to interact with different proteins, adsorption assays were conducted using bovine serum albumin (BSA) and lysozyme (Lyz) proteins, carefully chosen because of their different molecular weights and, especially, charges (BSA: M_w = 66.5 kDa, isoelectric point in water at 25 ºC = 4.7; Lyz: M_w = 14.3 kDa; isoelectric point = 11.3). Three replicates of PLA and PEDOT films supported on steel, 5-pPLA/CP_{AP} FsNMs and bare steel sheets (used as control) were immersed during 24 hours in a 0.5 mg/mL BSA or Lyz protein solution.

Figure 6a display the protein concentration onto the different surfaces measured by Bradford protein assay. As can be seen, the adsorption of both BSA and Lyz proteins was significantly higher on the FsNMs than on PLA and PEDOT films and the control. This has been attributed to the surface roughness (Rq= 103±9, 6±1, 376±34 and 11±2 nm for

5-pPLA/CP_{AP}, PLA, PEDOT and steel, respectively), which intrinsically favors the adherence of not only small proteins, like Lyz, but also of large biomolecules, such as BSA. Moreover, as it was expected, 5p-PLA/CP_{AP} FsNMs are highly selective favoring the adsorption of the most charged protein, Lyz. Thus, oxidized PEDOT chains located at the nanoperforations prefer charge proteins while non-polar PLA tends to adsorb both BSA and Lyz. Consequently, the amount of Lyz is 56% higher than that of BSA. These results indicate that the combination of surface roughness and the controlled distribution of PEDOT chains, which can be regulated through the size of the nanoperforations (*i.e.* by the composition of the PLA:PVA mixture) [11], is a suitable strategy for the separation of charged proteins.

These results were corroborated using gel electrophoresis assays. The electrophoretogram of the proteins adhered onto the 5-pPLA/CP_{AP} FsNMs is display in Figure 6b. Lane 2 and 3 shows a typical band corresponding to the a BSA control and the proteins adhered to 5-pPLA/CP_{AP} after 24 of incubation. Similar results were observed in Lane 4 and 5 which correspond to Lyz control and sample, meanwhile, the Lane 6 exhibit both bands (BSA and Lyz) as a result of the incubation in the presence of both proteins.

Electroactivity of 5-pPLA/CP_{AP} FsNMs

CPs are considered smart materials in the world of biomedicine since they allow electrical and electrochemical stimulation for the detection of bioanalytes, the controlled release of drug or in the transport of signal through neural implants, among others [44]. From a biotechnological point of view, CPs not only appropriate to stimulate nerve cells, which are specialized in receiving and transmit electrical stimuli, but also to enhance the viability of conventional cell types without the need of externally controlled stimuli [10,29,44,45]. This has been typically attributed to the intrinsic ability of CPs to

exchange ions with the cell through its membrane, enhancing of the cell metabolism and promoting cell adhesion and proliferation. The ability of CPs to exchange ions is measured by determining their electrochemical activity, which evaluates the facility of dopant ions to access and escape from the polymeric matrix upon oxidation and reduction processes, respectively.

Figure 7a displays the control cyclic voltammogram recorded for the 5-pPLA/CP_{AP} FsNMs membrane in a three-electrode cell with PBS 0.1M (pH 7.4) as electrolyte solution. The electroactivity, which is estimated from the area of the voltammogram, remains practically unaltered after 20 consecutive oxidation-reduction cycles, as is evidenced by the overlapping with the control voltammogram (Figure 7a). These results have been attributed to the conducting channels created by PEDOT layers, which can be appreciated as light shadows below PLA outer layer in the SEM micrographs shown in Figures 2c and 2e.

On the other hand, the effect produced by the adsorption of proteins in the electrochemical activity of the 5-pPLA/CP_{AP} FsNMs is displayed in Figure 7b. As it was expected, the area of the voltammograms decreased significantly after the adsorption of BSA and, especially, Lyz. Moreover, the reduction of the cathodic current density at the initial/final potentials is more pronounced when the adsorbed protein is Lyz than BSA, even though it noticeable for both proteins. These results are consistent with the higher affinity of the CP phases, which are accessible through the nanoperforations of the outer PLA layer, towards Lyz, supporting the observations reported in Figure 6.

CONCLUSIONS

Although electropolymerized PEDOT presents excellent properties (*e.g.* high electrochemical activity and environmental stability), its mechanical consistency is null, disintegrating into powder when the film is detached from the support used as working electrode in the AP process. In this work we propose a new strategy to produce flexible, robust and electroactive free-standing multilayered films combining PLA, which provides mechanical strength, and *in situ* electropolymerized PEDOT. The novelty of this approach lies in: (1) the semiconducting nature of the PEDOT:PSS sacrificial layer, and (2) the nanoperforations of the PLA layers, which enable the access of EDOT monomers to the semiconducting sacrificial layer or to the previously electropolymerized PEDOT layer. The synergistic interaction between the two polymers plays a pivotal role in 5-pPLA/CP_{AP}, which preserve the mechanical properties of PLA and the good electrochemical activity of PEDOT. Finally, cell culture and protein adsorption assays have shown that 5-pPLA/CP_{AP} FsNMs behave as bioactive platforms for cell proliferation and as bioadhesive surfaces for protein separation, respectively. It is expected that, after further optimization, 5-pPLA/CP_{AP} films will be suitable for many other promising technological applications due to the advantageous properties of their two components.

SUPPORTING INFORMATION

Synthetic methods and characterization techniques. Figures S1-S4 as described in the text. This material is available free of charge via the internet at http://pubs.acs.org.

ACKNOWLEDGEMENTS

This work was supported by MINECO (MAT2015-69367-R) and the Agència de Gestió d'Ajuts Universitaris i de Recerca (2017SGR359). Support for the research of C.A. was received through the prize "ICREA Academia" for excellence in research funded by the Generalitat de Catalunya. B.G.M. is thanked to CONACYT for the financial support through a postgraduate scholarship (328467 CVU 621314).

DATA AVAILABILITY

The raw/processed data required to reproduce these findings are available upon request to the authors.

REFERENCES

[1] S. Mitragotri, D. G. Anderson, X. Y. Chen, E. K. Chow, D. Ho, A. V. Kabanov, J. M. Karp, K. Kataoka, C. A. Mirkin, S. H. Petrosko, J. J. Shi, M. M. Stevens, S. H. Sun, S. Teoj, S. S. Venkatraman, Y. N. Xia, S. T. Wang Z. Gu, C. J. Xu, Accelerating the translation of nanomaterials in biomedicine, ACS Nano 9 (2015) 6644–6654.

[2] Teradal, N. L., Jelinek, R. 2017. Carbon nanomaterials: Carbon nanomaterials in biological studies and biomedicine, Adv. Healthc. Mater. 6, 1700574.

[3] X. Yang, M. Yang, B. Pang, M. Vara, Y. Xia, Gold nanomaterials at work in biomedicine, Chem. Rev. 115 (2015) 10410–10488.

[4] S. Fleischer, T. Dvir, Tissue engineering on the nanoscale: Lessons from the heart, Curr. Opin. Biotechnol. 24 (2013) 664–671.

[5] T. Cohen-Karni, R. Langer, D. S. Kohane, The smartest materials: The future of nanoelectronics in medicine, ACS Nano 6 (2012) 6541–6545.

[6] J. D. Kittle, C. Wang, C. Qian, Y. Zhang, M. Zhang, M. Roman, J. R. Morris, R. B. Moore, A. R. Esker, Ultrathin chitin films for nanocomposites and biosensors, Biomacromolecules 13 (2012) 714–718.

[7] ElAfandy, R. T., AbuElela, A. F., Mishra, P., Janjua, B., Oubei, H. M., Buttner, U., Majid, M. A., Ng, T. K., Merzaban, J. S., Ooi, B. S. 2017. Nanomembrane-based, thermal-transport biosensor for living cells. Small 13, 1603080.

[8] D. Son, J. Lee, S. Qiao, R. Ghaffari, J. Kim, J. E. Lee, C. Song, S. J. Kim, D. J. Lee, S. W. Jun, S. Yang, M. Park, J. Shin, K. Do, M. Lee, K. Kang, C. S. Hwang, N. S. Lu, T. Hyeon, D. H. Kim, Multifunctional wearable devices for diagnosis and therapy of movement disorders, Nat. Nanotech. 9 (2014) 397–404.

[9] C. S. Hajicharalambous, J. Lichter, W. T. Hix, M. Swierczewska, M. F. Rubner, P. Rajagopalan, Nano- and sub-micron porous polyelectrolyte multilayer assemblies: biomimetic surfaces for human corneal epithelial cells, Biomaterials 30 (2009) 4029–4036.

[10] M. M. Pérez-Madrigal, M. I. Giannotti, L. J. del Valle, L. Franco, E. Armelin, J. Puiggalí, F. Sanz, C. Alemán, Thermoplastic polyurethane:polythiophene nanomembranes for biomedical and biotechnological applications, ACS Appl. Mater. Interfaces 6 (2014) 9719–9732.

[11] A. Puiggalí-Jou, J. Medina, L. J. del Valle, C. Alemán, Nanoperforations in poly(lactic acid) free-standing nanomembranes to promote interactions with cell filopodia, Eur. Polym. J. 75 (2016) 552–564.

[12] Z. Tai, H. Ma, B. Liu, X. Yan, Q. Xue, Facile synthesis of Ag/GNS-g-PAA nanohybrids for antimicrobial applications, Colloids Surf. B 89 (2012) 147–151.

[13] S. Y. Wong, Q. Li, J. Veselinovic, B.-S. Kim, A. M. Klibanov, P. T. Hammond, Bactericidal and virucidal ultrathin films assembled layer by layer from

polycationic N-alkylated polyethylenimines and polyanions. Biomaterials 31 (2010) 4079–4087.

[14] M. M. Pérez-Madrigal, E. Llorens, L. J. del Valle, J. Puiggalí, E. Armelin, C. Alemán, Semiconducting, biodegradable and bioactive fibers for drug delivery, Express Polym. Lett. 10 (2016) 628–646.

[15] A. Albisa, L. Español, M. Prieto, V. Sebastian, Polymeric nanomaterials as nanomembrane entities for biomolecule and drug delivery, Curr. Pharm. Des. 23 (2017) 263–280

[16] H. Watanabe, E. Muto, T. Ohzono, A. Nakao, T. Kunitake, Giant nanomembrane of covalently-hybridized epoxy resin and silica, J. Mater. Chem. 19 (2009) 2425–2931.

[17] K. D. Sattler, Handbook of Nanophysics, Vol. 5. Functional Nanomaterials., CRC Press. Taylor and Francis Group, Boca Raton, FL 2011.

[18] T. Fujie, Development of free-standing polymer nanosheets for advanced Medical and health-care applications, Polym. J. 48 (2016) 773–780.

[19] M. M. Pérez-Madrigal, E. Armelin, J. Puiggalí, C. Alemán, Insulating and semiconducting polymeric free-standing nanomembranes with biomedical applications, J. Mater. Chem. B 3 (2015) 5904–5932.

[20] Zhang, S.; Sunami, Y.; Hashimoto, H. Mini Review: Nanosheet Technology towards Biomedical Application. *Nanomaterials* **2017**, *7*, 246.

[21] G. Decher, Fuzzy nanoassemblies: Toward layered polymeric multicomposites, Science 277 (1997) 1232–1237.

[22] G. Decher, Y. Lvov, J. Schmitt, Proof of multilayer structural organization in self-assembled polycation-polyanion molecular films, Thin Solid Films 244 (1994) 772–777.

[23] A. D. Stroock, R. S. Kane, M. Weck, S. J. Metallo, G. M. Whitesides, Synthesis of free-standing quasi-two-dimensional polymers, Langmuir 19 (2003) 2466–2472.

[24] Y. Okamura, K. Kabata, M. Kinoshita, H. Miyazaki, A. Saito, T. Fujie, S. Ohtsubo, D. Saitoh, S. Takeoka, Fragmentation of poly(lactic acid) nanosheets and patchwork treatment for burn wounds, Adv. Mater. 25 (2013**)** 545–551.

[25] J. Stana, J. Stergar, L. Gradinik, V. Flis, R. Kargl, E. Fröhlich, K. S. Kleinschek, T. Mohan, U. Maver, Multilayered polysaccharide nanofilms for controlled delivery of pentoxifylline and possible treatment of chronic venous ulceration, Biomacromolecules 18 (2017) 2732−2746.

[26] S. Kim, J. M. Moon, J. S. Choi, W. K. Cho, M. S. Kang, Mussel-inspired approach to constructing robust multilayered alginate films for antibacterial applications, Adv. Funct. Mater. 26 (2016) 4099−4105.

[27] C. Ferris, M. V. de Paz, A. Aguilar de Leyva, I. Caraballo, J. A. Galbis, Reduction-sensitive functionalized copolyurethanes for biomedical applications, Polym. Chem. 5 (2014) 2370−2381.

[28] W. C. Liu, H. Y. Wang, A. N. Wang, C. H. Teng, H. L. Liu, R. J. Chung, 2017. Preparation of chitosan/poly-gamma-glutamic acid polyelectrolyte multilayers on biomedical metals for local antibiotic delivery, Metals. 7, 418.

[29] L. Groenendaal, G. Zotti, P.-H. Aubert, S. M. Waybright, J. R. Reynolds, Electrochemistry of poly(3,4-alkylenedioxythiophene) derivatives, Adv. Mater. 15 (2003) 855−879.

[30] S. Kirchmeyer, K. Reuter, Scientific importance, properties and growing applications of poly(3,4-ethylenedioxythiophene), J. Mater. Chem. 15 (2005) 2077−2088.

[31] L. J. del Valle, F. Estrany, E. Armelin, R. Oliver, C. Alemán, Cellular adhesion, proliferation and viability on conducting polymer substrates, Macromol. Biosci. 8 (2008) 1144−1151.

[32] A. Puiggalí-Jou, P. Micheletti, L. J. del Valle, C. Alemán, 2017. Electrostimulated release of neutral drugs from polythiophene nanoparticles: Smart regulation of drug–polymer interactions. Adv. Healthcare Mater. 6, 1700453.

[33] A. Puiggalí-Jou, M. M. Pérez-Madrigal, L. J. del Valle, E. Armelin, M. T. Casas, C. Michaux, E. A. Perpéte, F. Estrany, C. Alemán, Confinement of a β-barrel protein in nanoperforated free-standing nanomembranes for ion transport, Nanoscale 8 (2016) 16922−16935.

[34] . Fujie, L. Ricotti, A. Desii, A. Menciassi, P. Dario, V. Mattoli, Evaluation of substrate effect on cell adhesion properties using freestanding poly(l-lactic acid) nanosheets, Langmuir 27 (2011) 13173−13182.

[35] Y. Okamura, K. Kabata, M. Kinoshita, D. Saitoh, S. Takeoka, Free-standing biodegradable poly(lactic acid) nanosheet for sealing operations in surgery, Adv. Mater. 21 (2009) 4388−4392.

[36] H. Miyazaki, M. Kinoshita, A. Saito, T. Fujie, K. Kabata, E. Hara, S. Ono, S. Takeoka, D. Saitoh, An ultrathin poly(L-lactic acid) nanosheet as a burn wound dressing for protection against bacterial infection, Wound Repair Regen. 20 (2012) 573−579.

[37] V. Pensabene, S. Taccola, L. Ricotti, G. Ciofani, A. Menciassi, F. Perut, M. Salermo, P. Dario, N. Baldini, Flexible polymeric ultrathin film for mesenchymal stem cell differentiation, Acta Biomater. 7 (2011) 2883−2891.

[38] X. Punet, R. Mauchauffe, M. I. Giannotti, J. C. Rodríguez-Cabello, F. Sanz, E. Engel, M. A. Mateos-Timoneda, J. A. Planell, Enhanced cell-material interactions

through the biofunctionalization of polymeric surfaces with engineered peptides, Biomacromolecules 14 (2013) 2690−2692.

[39] R. A. Auras, L.-T. Lim, S. E. M. Selke, H. Tsuji, Poly(lactic acid): Synthesis, structures, properties, processing, and applications, John Wiley & Sons, New Jersey, 2011.

[40] Y.-K. Han, M.-Y. Chang, W.-Y. Huang, H.-Y. Pan, K.-S. Ho, T.-H. Hsieh, S.-Y. Pan, Improved performance of polymer solar cells featuring one-dimensional PEDOT nanorods in a modified buffer layer, J. Electrochem. Soc. 158 (2011) K88−K93.

[41] A. A. Farah, S. A. Rutledge, A. Schaarschmidt, R. Lai, J. P. Freedman, A. S. Helmy, 2012. Conductivity enhancement of poly(3,4-ethylenedioxythiophene)-poly(styrenesulfonate) films post-spincasting, J. Appl. Phys. 112, 113709.

[42] A. Shakoor, T. Z. Rizvi, Raman spectroscopy of conducting poly(methylmethacrylate)/polyaniline-dodecylbenzenesulfonate blends, J. Raman Spectrosc. 41 (2010) 237−240.

[43] R. V. Salvatierra, L. G. Moura, M. M. Oliveira, M. A. Pimienta, A. J. G. Zarbin, Resonant Raman spectroscopy and spectroelectrochemistry characterization of carbon nanotubes/polyaniline thin film obtained through interfacial polymerization, J. Raman Spectrosc. 43 (2012) 1094−1100.

[44] . Balint, N. J. Cassidy, S. H. Cartmell, Conductive polymers: Towards a smart biomaterial for tissue engineering, Acta Biomater. 10 (2014) 2341−2353.

[45] K. J. Gilmore, M. Kita, Y. Han, A. Gelmi, M. J. Higgins, S. E. Moulton, G. M. Clark, R. Kapsa, G. G. Wallace, Skeletal muscle cell proliferation and differentiation on polypyrrole substrates doped with extracellular matrix component. Biomaterials 30 (2009) 5292−5304.

CAPTIONS TO FIGURES

Figure 1. (a) Scheme displaying the three-step procedure used to prepare the nanoperforated PLA films: (1) dropping of the 90:10 PLA-PVA mixture onto a steel substrate; (2) spin-coating of the PLA-PVA mixture; and (3) etching of PVA using milli-Q water. (b) Scheme illustrating the preparation of 5-pPLA/CP_{AP} films. This consists in the alternation of perforated PLA layers, which were prepared as described in (a), and the deposition of PEDOT layers by AP.

Figure 2. High resolution SEM micrograph (left), 3D topographic and height AFM images (center and right, respectively) of each layer in 5-pPLA/CP_{AP} films: (a) 1st PLA layer; (b) 2nd PEDOT layer; (c) 3rd PLA layer; (d) 4th PEDOT layer; and (e) 5th PLA layer.

Figure 3. (a) SEM micrograph showing the two sides of an intentionally scratched 2-layered film made by electropolymerizing EDOT onto a spin-coated PLA layer with nanoperforations. (b) Root-mean-square roughness (Rq), (c) thickness and (d) water contact angle (WCA) of each layer in 5-pPLA/CP_{AP} films. The thickness was determined by both profilometry and AFM scratching.

Figure 4. Digital camera images displaying: (a) a 5-pPLA/CP_{AP} film growing layer-by-layer (layer 0 refers to the sacrificial PEDOT:PSS layer); (b) a supported 5-pPLA/CP_{AP} film with area of 1×1 cm^2; (c) a free standing 5-pPLA/CP_{AP} film floating in water (left), its aspiration into a pipette (center) and the aspect of the film when it released from the pipette, recovering its initial shape. (d) Raman spectra of the 5-pPLA/CP_{AP} films as it grows layer-by-layer.

Figure 5. MTT evaluation of Cos-1 and Vero cells cultured on steel sheets (control), PLA and PEDOT films supported on steel, and free-standing 5-pPLA/CP_{AP} films for (a) 24 hours and (b) 7 days. Values are the mean and bars indicate their standard deviation.

(c) Micrographs of the Cos-1 and Vero cells cultured on the different substrates after 24 hours and 7 days.

Figure 6. (a) Adsorption (in %) of BSA and Lyz onto the surface of bare steel (control), PLA and PEDOT films supported on steel, and free standing 5-pPLA/CP_{AP} films after incubation for 24 h at room temperature. Values are the mean and bars indicate their standard deviation. The asterisk (∗) indicates a significant difference with the control when the Student's T-test is applied ($p < 0.05$). (b) Electrophoretogram showing: the nanomembrane as a control (lane 1); BSA reference (lane2); BSA adsorption onto 5-pPLA/CP_{AP} FsNM (lane 3); Lyz reference (lane 4); Lyz adsorption onto 5-pPLA/CP_{AP} FsNM (lane 5); BSA and Lyz adsorption onto 5-pPLA/CP_{AP} FsNM (lane 6).

Figure 7. (a) First control voltammogram (solid black line) and voltammogram after 20 consecutive oxidation–reduction cycles (dashed red line) for 5-pPLA/CP_{AP} FsNMs. The voltammogram of control PLA is displayed in grey. (b) Cyclic voltammogram recorded for the 5-pPLA/CP_{AP} FsNMs after 24 h incubation in 0.5 mg/mL BSA (dotted blue line) or Lyz (dashed purple line) protein solution. In all cases, voltammograms were recorded in a 0.1 M PBS solution (pH 7.4) using a scan rate of 100 mV/s. Initial and final potentials: -0.20V; reversal potential: +0.60 V.

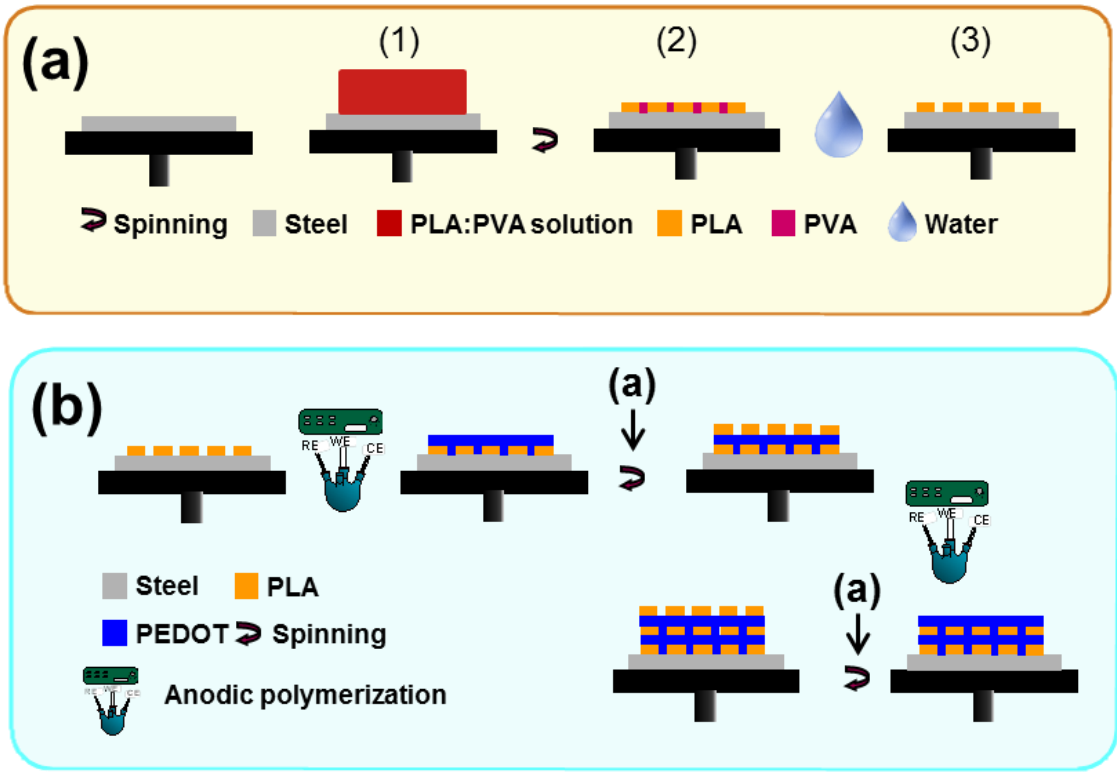
(a)
(1)
(2)
(3)
Spinning
Steel
PLA:PVA solution
PLA
PVA
Water
(b)
RE
WE
CE
(a)
Steel
PLA
PEDOT
Spinning
Anodic polymerization

Figure 1

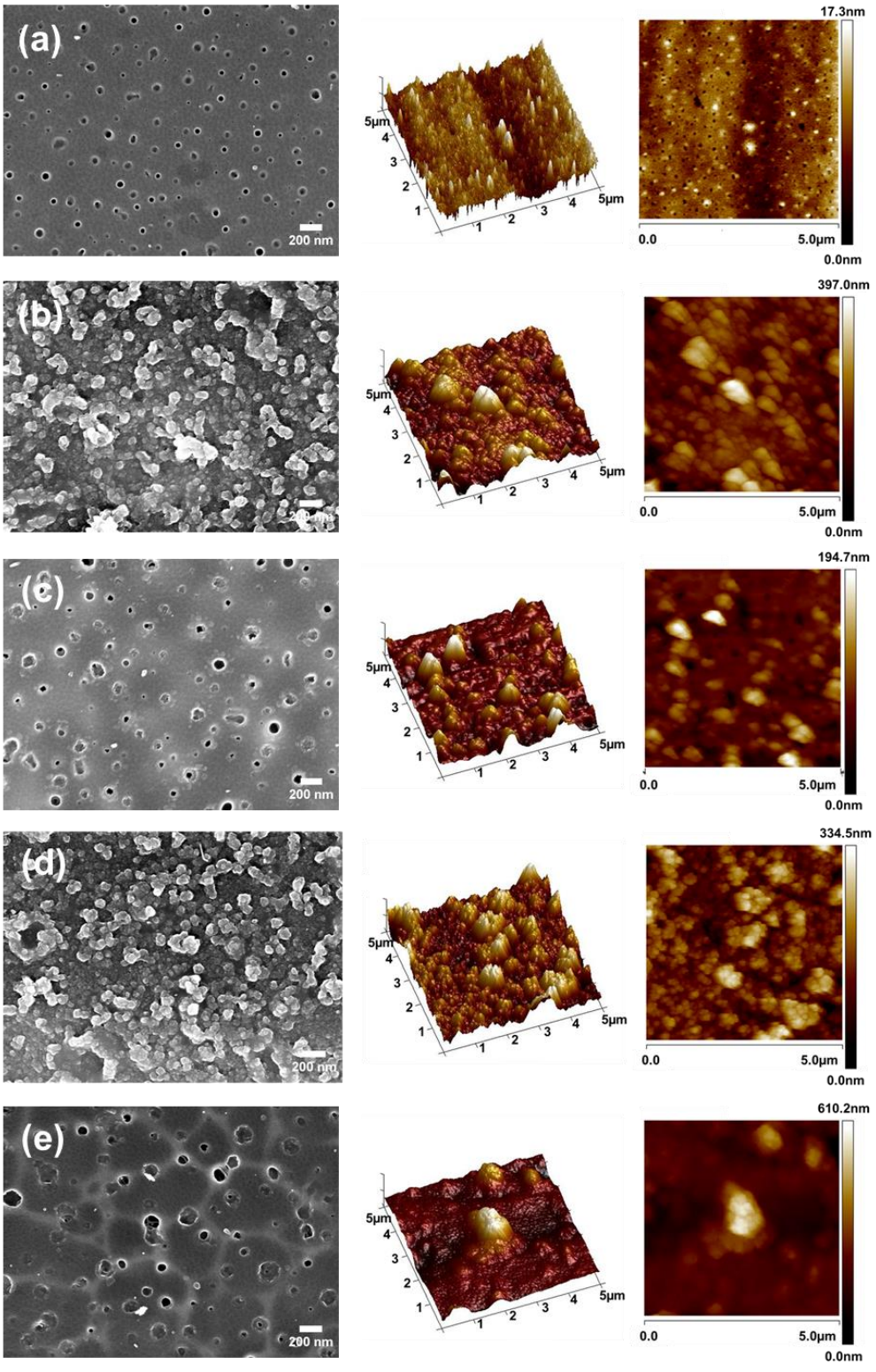
(a)
200 nm
5μm
4
3
2
1
1
2
3
4
5μm
17.3nm
0.0
5.0μm
0.0nm
(b)
200 nm
5μm
4
3
2
1
1
2
3
4
5μm
397.0nm
0.0
5.0μm
0.0nm
(c)
200 nm
5μm
4
3
2
1
1
2
3
4
5μm
194.7nm
0.0
5.0μm
0.0nm
(d)
200 nm
5μm
4
3
2
1
1
2
3
4
5μm
334.5nm
0.0
5.0μm
0.0nm
(e)
200 nm
5μm
4
3
2
1
1
2
3
4
5μm
610.2nm
0.0
5.0μm
0.0nm

Figure 2

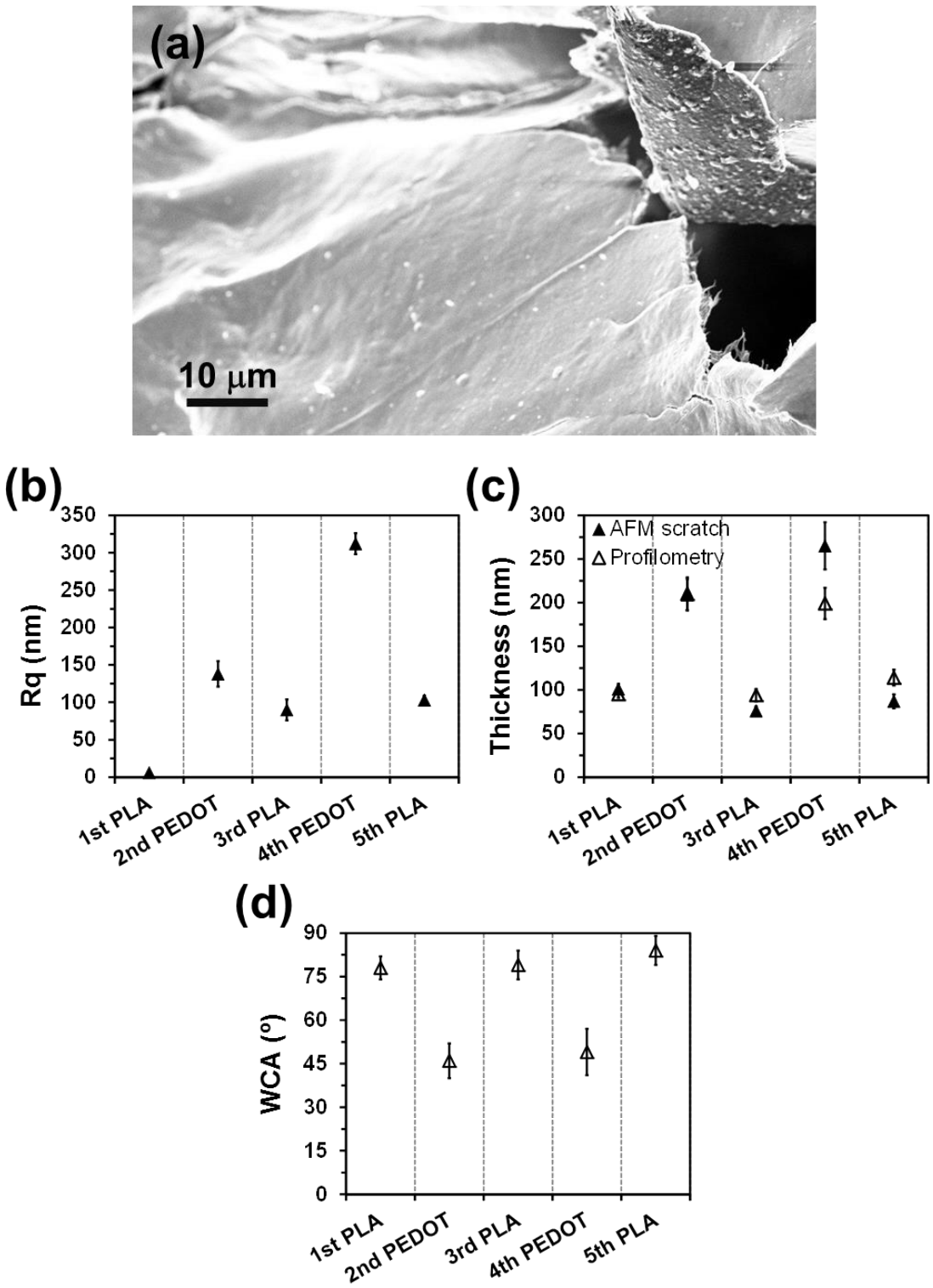
(a)
10 μm
(b)
Rq (nm)
0
50
100
150
200
250
300
350
1st PLA
2nd PEDOT
3rd PLA
4th PEDOT
5th PLA
(c)
Thickness (nm)
AFM scratch
Profilometry
0
50
100
150
200
250
300
1st PLA
2nd PEDOT
3rd PLA
4th PEDOT
5th PLA
(d)
WCA (°)
0
15
30
45
60
75
90
1st PLA
2nd PEDOT
3rd PLA
4th PEDOT
5th PLA

Figure 3

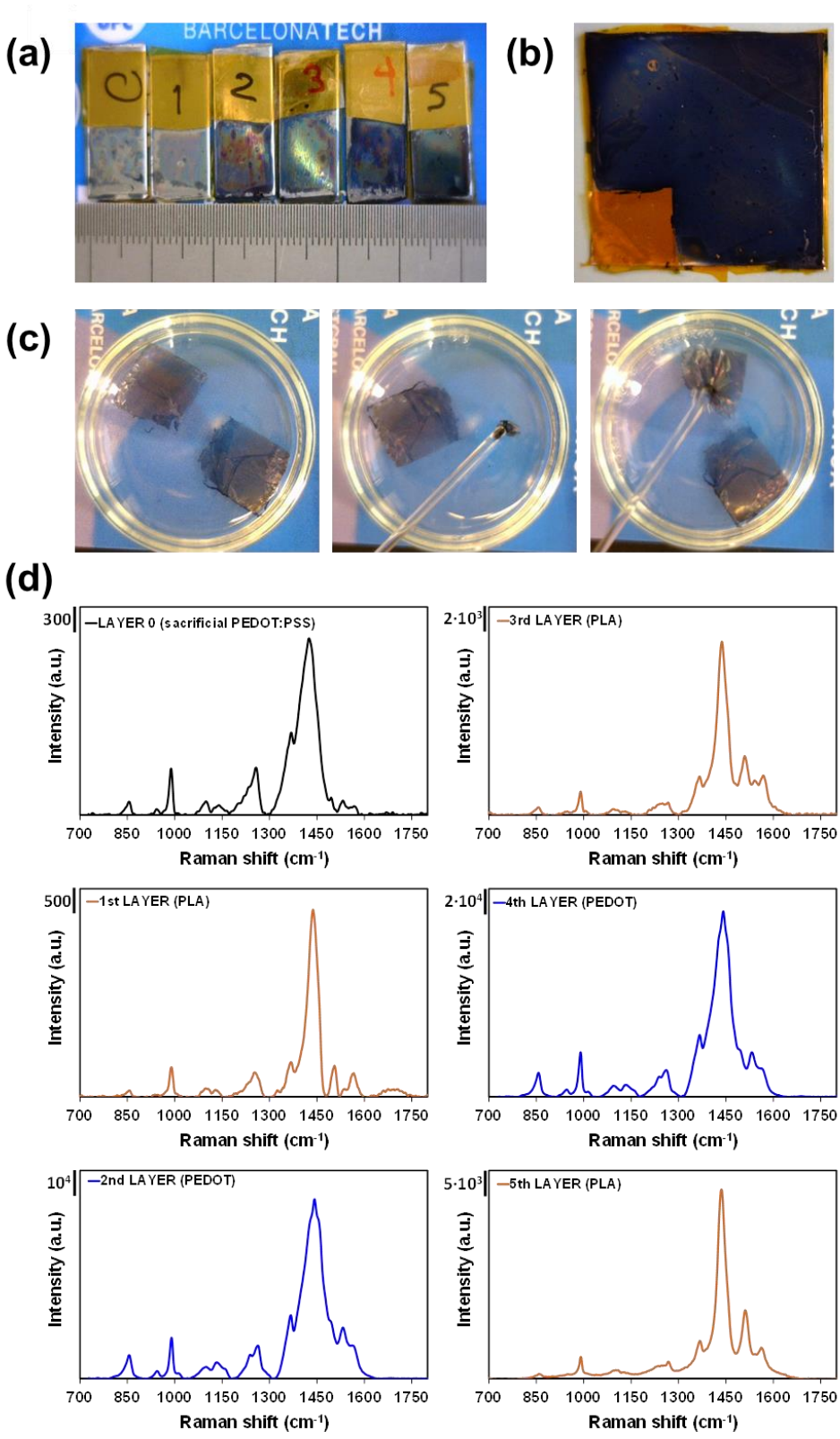
(a)
BARCELONATECH
0
1
2
3
4
5
(b)
(c)
(d)
LAYER 0 (sacrificial PEDOT:PSS)
3rd LAYER (PLA)
1st LAYER (PLA)
4th LAYER (PEDOT)
2nd LAYER (PEDOT)
5th LAYER (PLA)
Intensity (a.u.)
Raman shift (cm-1)
700 850 1000 1150 1300 1450 1600 1750

Figure 4

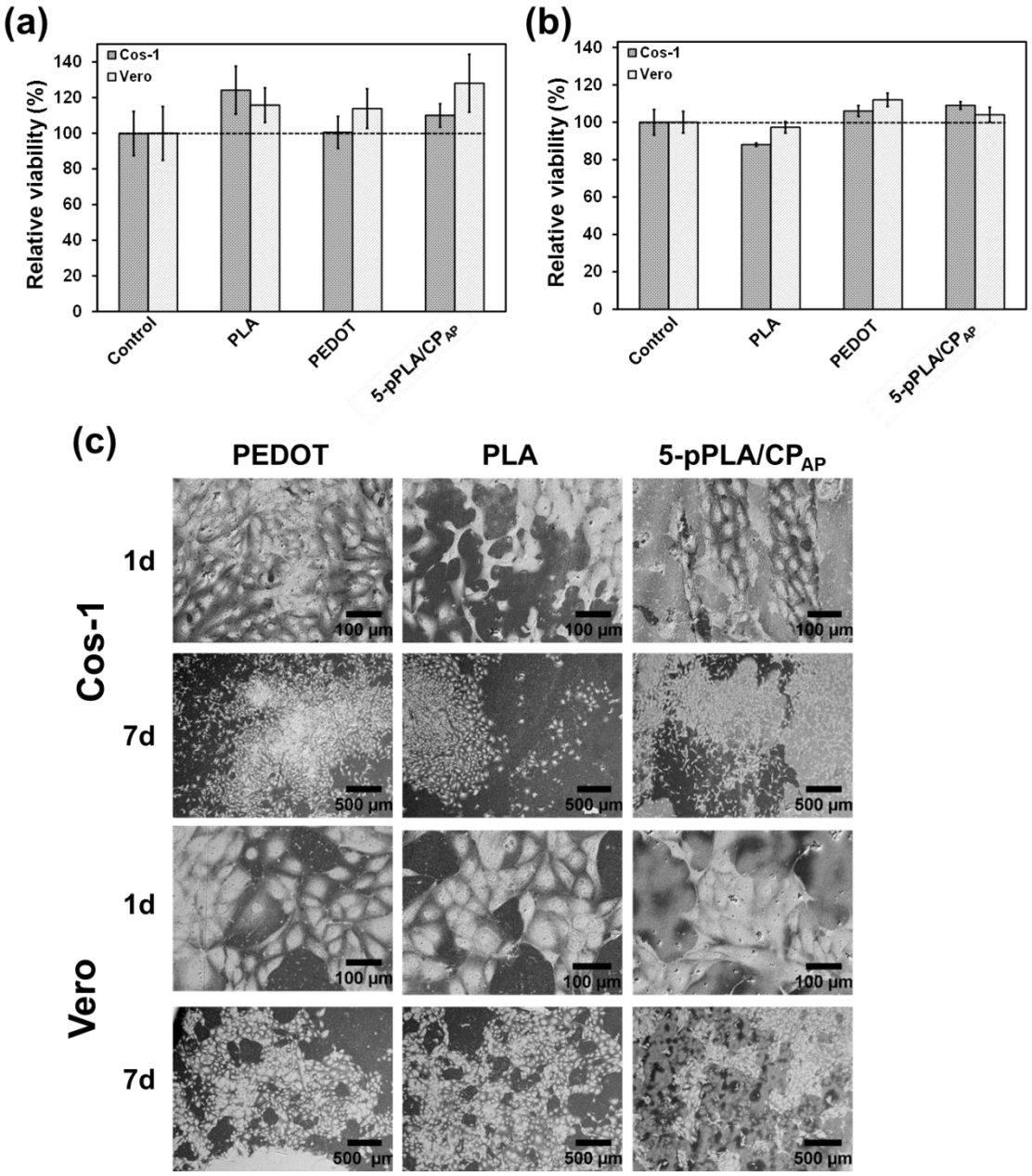
(a)
Cos-1
Vero
Relative viability (%)
0
20
40
60
80
100
120
140
Control
PLA
PEDOT
5-pPLA/CP$_{AP}$
(b)
Cos-1
Vero
Relative viability (%)
0
20
40
60
80
100
120
140
Control
PLA
PEDOT
5-pPLA/CP$_{AP}$
(c)
PEDOT
PLA
5-pPLA/CP$_{AP}$
Cos-1
1d
7d
Vero
1d
7d
100 μm
500 μm

Figure 5

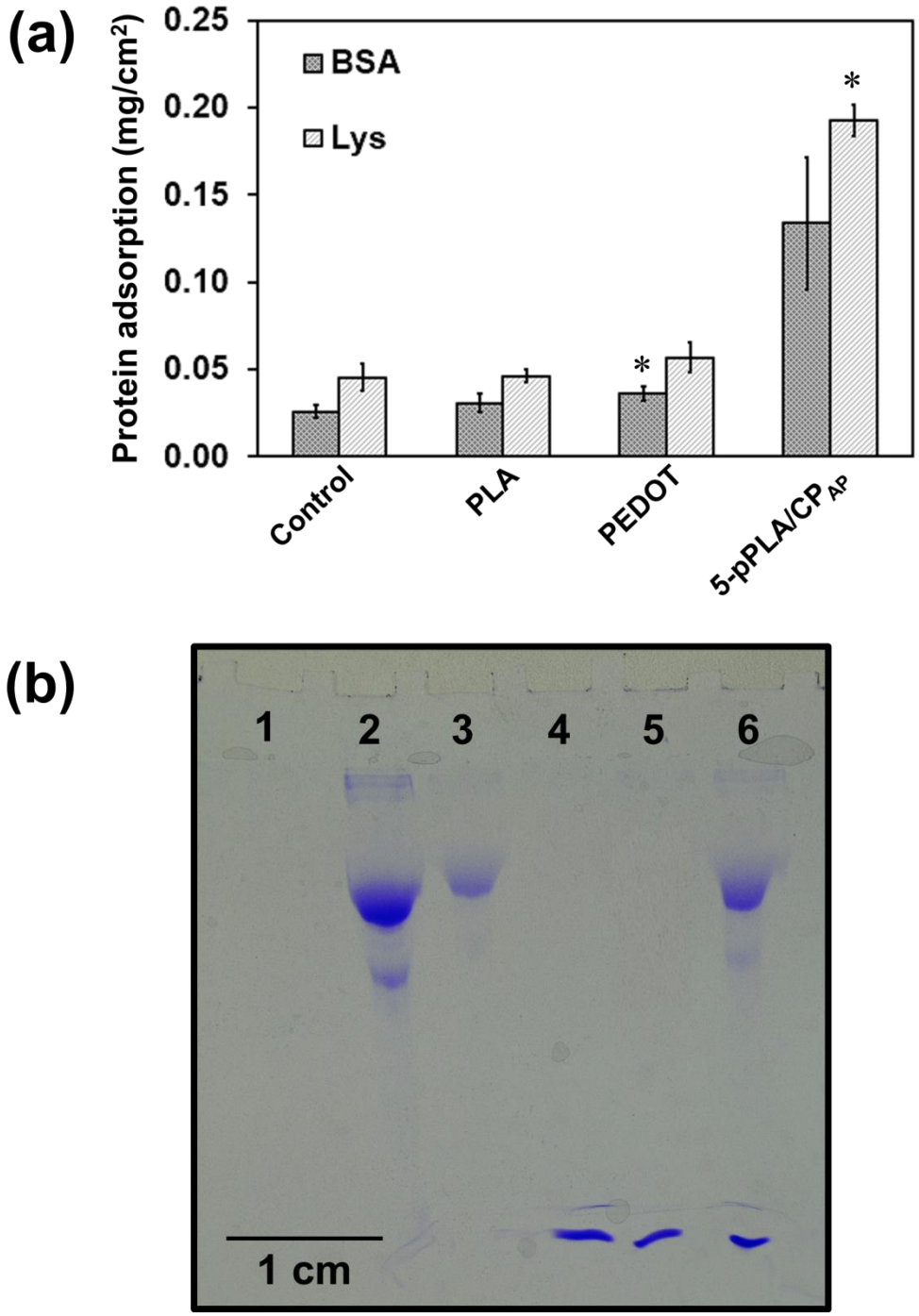
(a)
Protein adsorption (mg/cm²)
0.25
0.20
0.15
0.10
0.05
0.00
BSA
Lys
*
*
Control
PLA
PEDOT
5-pPLA/CP AP
(b)
1
2
3
4
5
6
1 cm

Figure 6

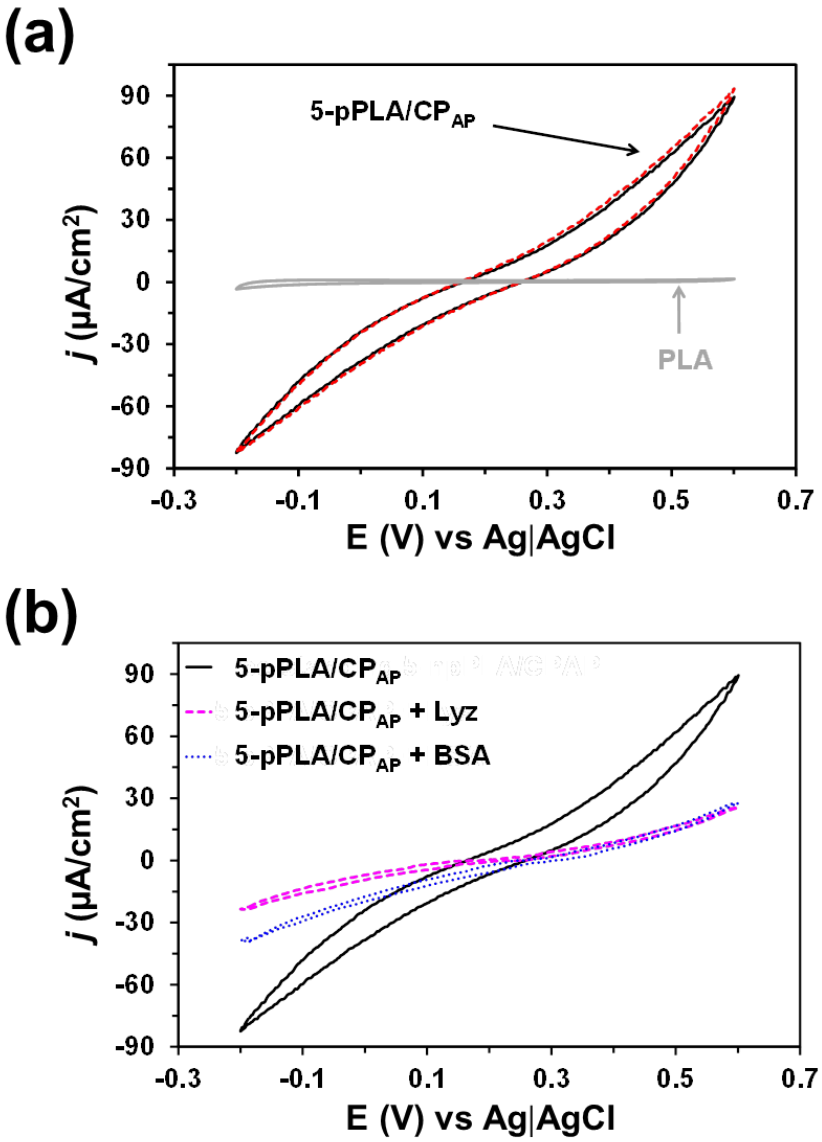
(a)
5-pPLA/CP$_{AP}$
PLA
j (μA/cm^2)
E (V) vs Ag|AgCl
(b)
5-pPLA/CP$_{AP}$
5-pPLA/CP$_{AP}$ + Lyz
5-pPLA/CP$_{AP}$ + BSA
j (μA/cm^2)
E (V) vs Ag|AgCl

Figure 7